Electronic Supplementary Material (ESI) for Nanoscale.

Supporting Information

High-Efficiency All Fluorescence White OLEDs with High Color Rendering Index by Manipulating Excitons in Co-host Recombination Layers

Yuan-Bo Zhang,[a] Ya-Nan Li,[a] Chun-Fang Zhang,[a] Jia-Bo Liu,[a] Jia-Rui Li,[a] Hao-Dong Bian,[a] Lian-Qing Zhu,[a] Jian-Zhen Ou,[b] Lin-Song Cui,*[c,d] Yuan Liu*[a]

1. Energy diagram and carrier transport behavior of single host and co-host devices

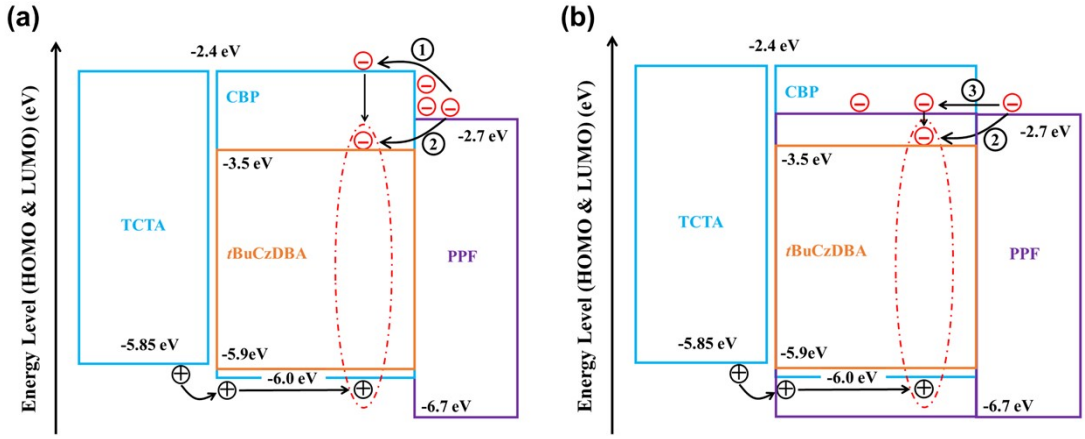

Fig. S1. Energy diagram and carrier transport behavior in (a) single-host system and (b) co-host system.

Taking yellow device Y1 as the example, there are two routes for electron injection with single-host (as shown in the Fig. S1a). The first route is direct injection into the host material CBP (route 1), which requires to overcome a high injection barrier due to the large difference between CBP and PPF. It is also possible to inject the electron from PPF to the emitter *t*BuCzDBA (route 2). However, due to only 10% doping ratio of the emitting molecules, this process (the route of "2") is not dominant. In the co-host CBP:PPF, as shown in Fig. S1b, electrons can directly inject from the exciton-blocking layer PPF to the light-emitting layer without injection barriers (the route of "3"). That means the co-host systems with PPF can reduce the barrier for electron injecting, which is the key to realizing lower turn-on voltages.

2. EL performance of mCBP based yellow devices

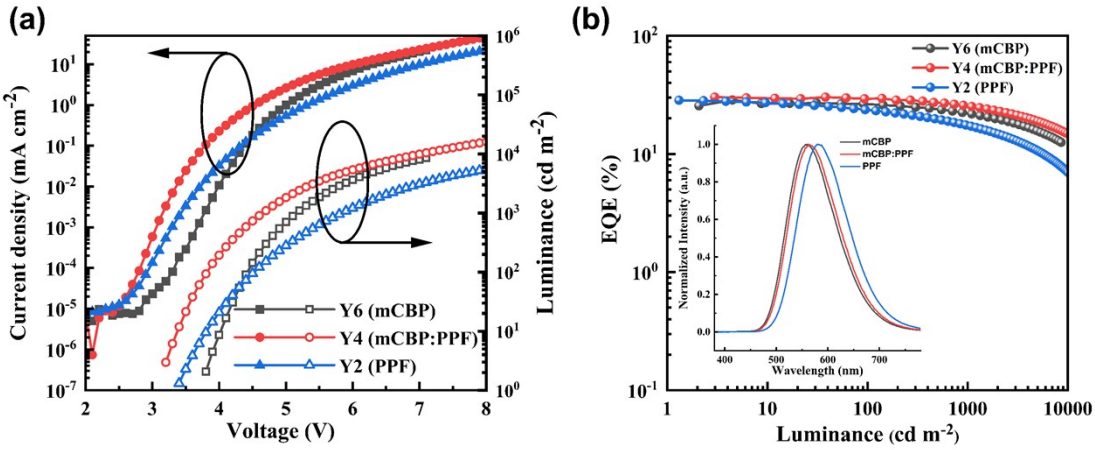

Fig. S2. (a) Current density-voltage-luminance characteristics of mCBP based yellow devices. (b) EQE-luminance curves of mCBP based yellow devices. Insets in panel (b): The normalized EL spectra of mCBP based yellow devices at 10 mA cm^{-2}.

3. EL performance of TCTA based yellow devices

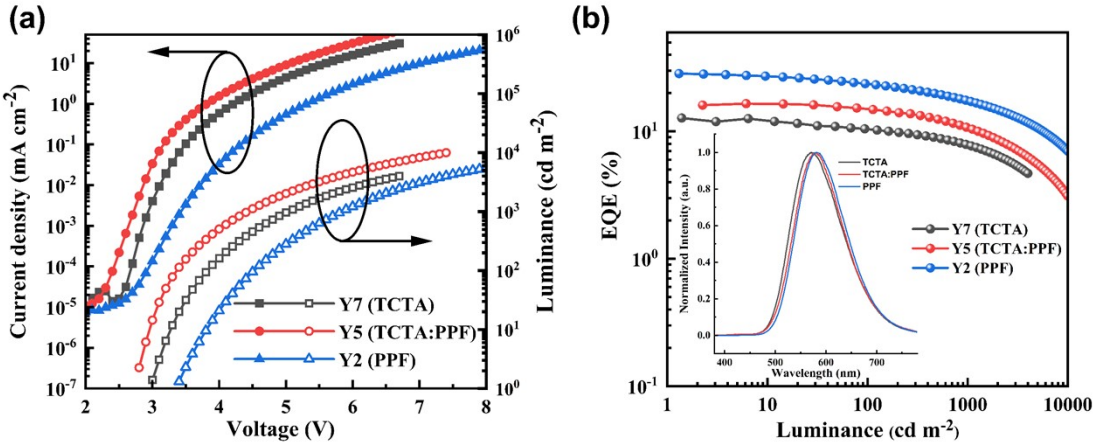

Fig. S3. (a) Current density-voltage-luminance characteristics of TCTA based yellow devices. (b) EQE-luminance curves of TCTA based yellow devices. Insets in panel (b): The normalized EL spectra of TCTA based yellow devices at 10 mA cm^{-2}.

4. PL spectra of hosts for yellow devices

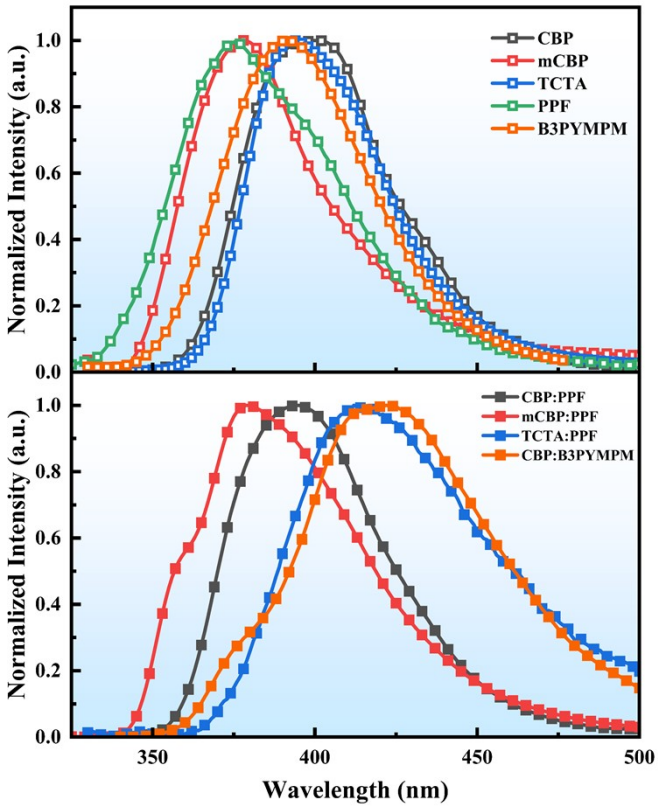

Fig. S4. PL spectra of neat and mixed films (weight ratio of 1:1).

5. EL performance of device Y8

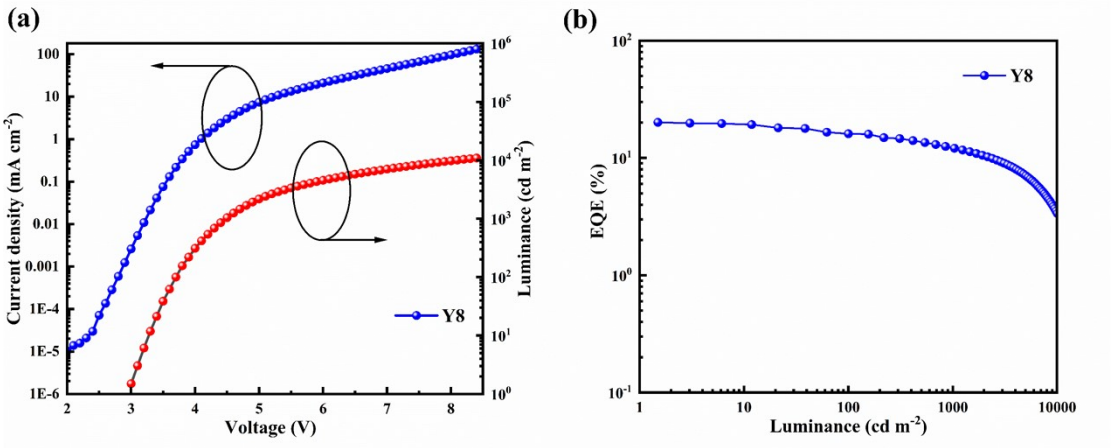

Fig. S5. (a) Current density-voltage-luminance characteristics of device Y8. (b) EQE-luminance curve of device Y8. Device Y8: ITO/HAT-CN (5 nm)/TAPC (40 nm)/TCTA (10 nm)/CBP:B3PYMPM:*t*BuCzDBA (1:1, 10%, 20 nm)/B3PYMPM (10 nm)/PBPPhen (50 nm)/Liq (2 nm)/Al (100 nm).

6. EL spectra of W2 and W3

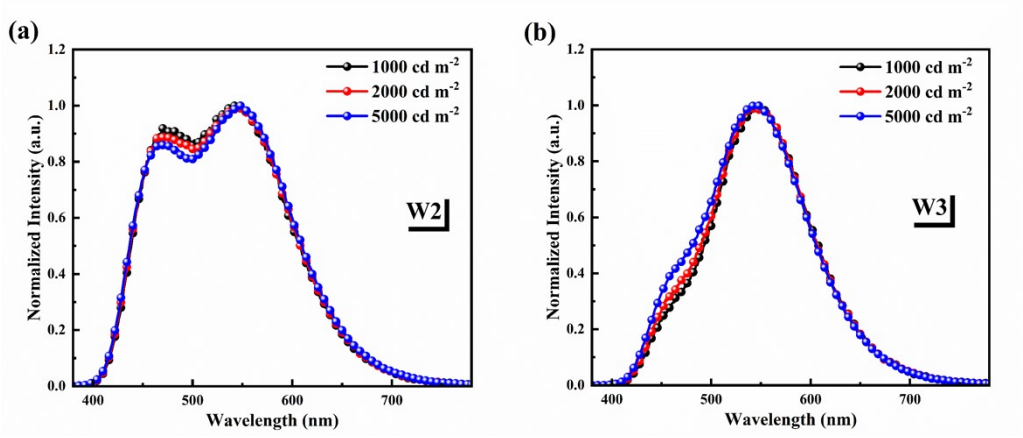

Fig. S6. EL spectra of (a) W2, and (b) W3 at 1000, 2000, and 5000 cd m^{-2}.

7. EL performance of device W4

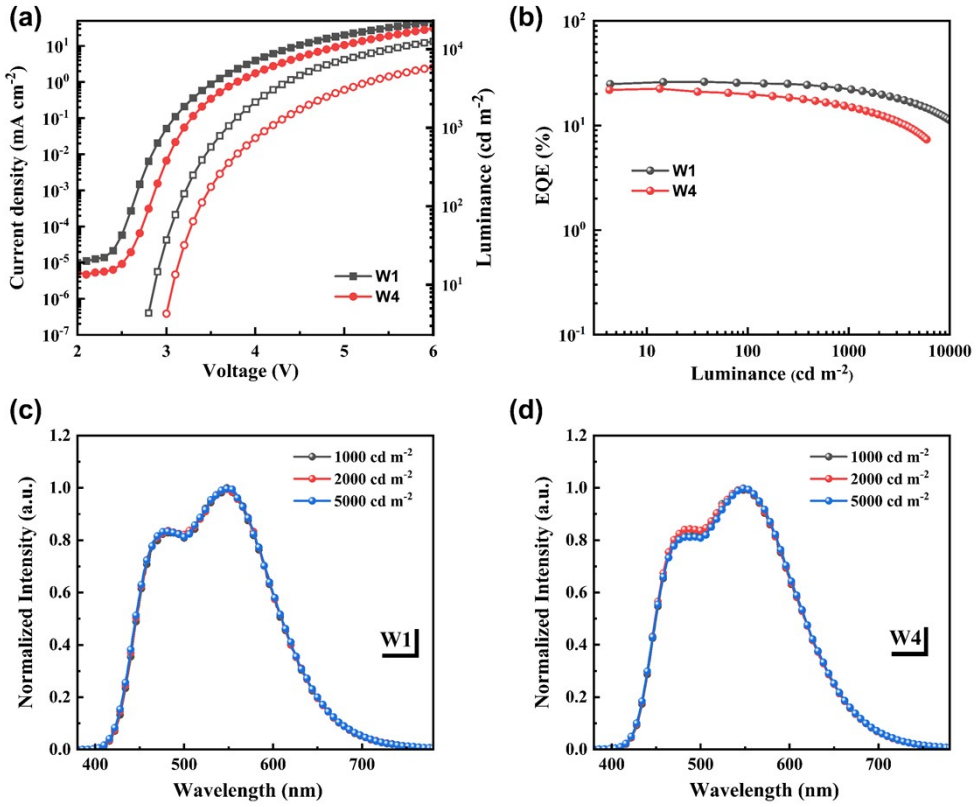

Fig. S7. (a) Current density-voltage-luminance characteristics of W1 and W4. (b) EQE versus luminance of W1 and W4. (c) The normalized EL spectra of W1 at 1000, 2000, and 5000 cd m^{-2}. (d) The normalized EL spectra of W4 at 1000, 2000, and 5000 cd m^{-2}.

8. Comparison of exciton recombination regions of W1 and W4

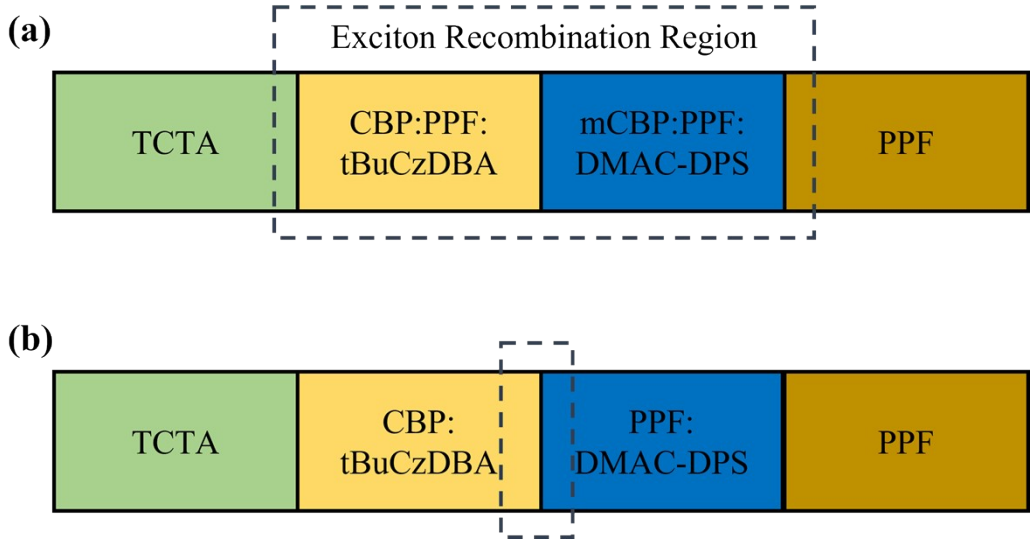

Fig. S8. Exciton recombination regions in devices (a) W1 and (b) W4 (Dashed box).

9. Investigation of exciton recombination region

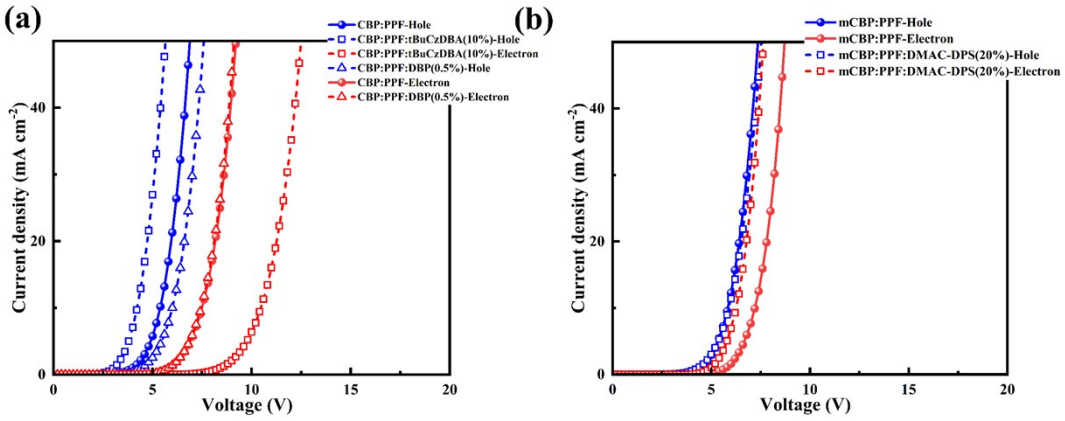

Fig. S9. Current density-voltage characteristics of single carrier devices.

The hole-only devices: ITO/HAT-CN (5 nm)/TAPC (40 nm)/TCTA (10 nm)/CBP:PPF (1:1, 20 nm), mCBP:PPF (1:1, 20 nm), CBP:PPF:DBP (1:1, 0.5%, 20 nm), CBP:PPF:*t*BuCzDBA (1:1, 10%, 20 nm), or mCBP:PPF:DMAC-DPS (1:1, 20%, 20 nm)/TAPC (20 nm)/HAT-CN (10 nm)/Al (100 nm).

The electron-only devices: ITO/Liq (2 nm)/PBPPhen (20 nm)/CBP:PPF (1:1, 20 nm), mCBP:PPF (1:1, 20nm), CBP:PPF:DBP (1:1, 0.5%, 20 nm), CBP:PPF:*t*BuCzDBA (1:1, 10%, 20 nm), or mCBP:PPF:DMAC-DPS (1:1, 20%, 20 nm)/PPF (10 nm)/PBPPhen (40 nm)/Liq (2 nm)/Al (100 nm).

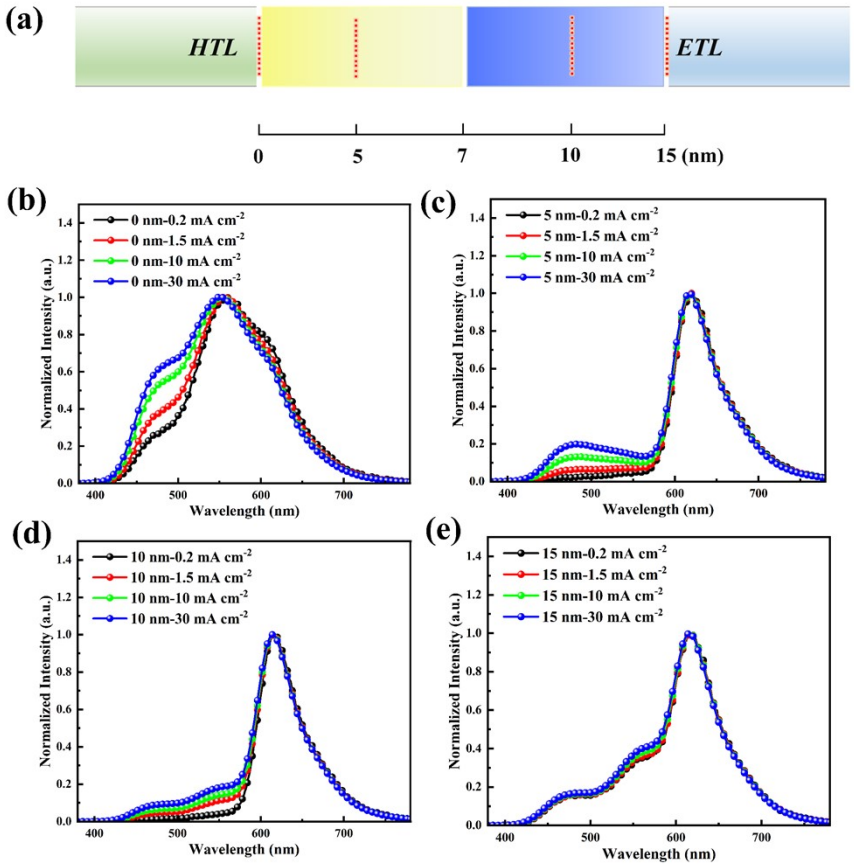

Fig. S10. Exciton allocation and distribution by inserting the ultrathin red phosphorescent interlayer (RD071, 0.1 nm) in different positions of the device W1. (a) positions of the red interlayer. (b)-(e) the EL spectra change within different positions at 0.2, 1.5, 10, and 30 mA cm^{-2}.

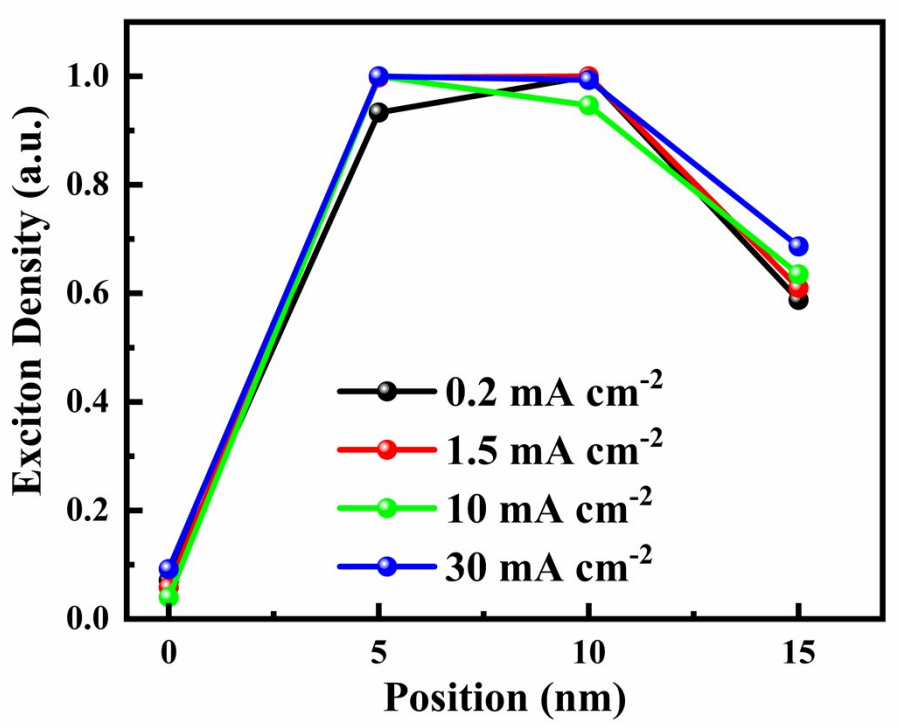

Fig. S11. The exciton densities at different positions 0, 5, 10, and 15 nm in the EML at 0.2, 1.5, 10, and 30 mA cm^{-2}.

10. EL performance of device W9

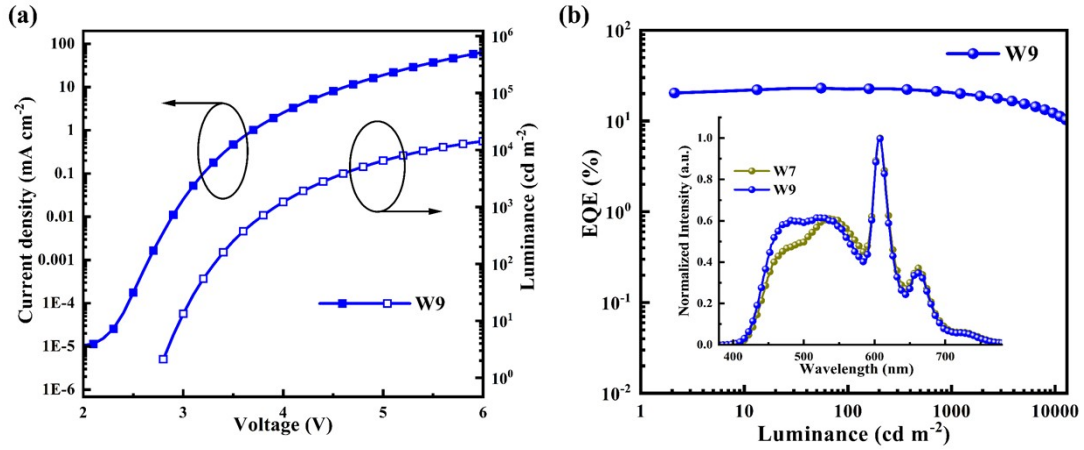

Fig. S12. (a) Current density-voltage-luminance characteristics. (b) EQE-luminance curve of W9. Insets in panel (b): The normalized EL spectra of W7 and W9 at 1000 cd m^{-2}. Device W9: ITO/HAT-CN (5 nm)/TAPC (40 nm)/TCTA (10 nm)/CBP:PPF:*t*BuCzDBA (1:1, 10%, 4 nm)/CBP:PPF:DBP (1:1, 0.5%, 3 nm)/CBP:PPF:*t*BuCzDBA (1:1, 10%, 4.5 nm)/mCBP:PPF:DMAC-DPS (1:1, 20%, 8 nm)/PPF (10 nm)/PBPPhen (50 nm)/Liq (2 nm)/Al (100 nm).

11. EL spectra of W5-W8

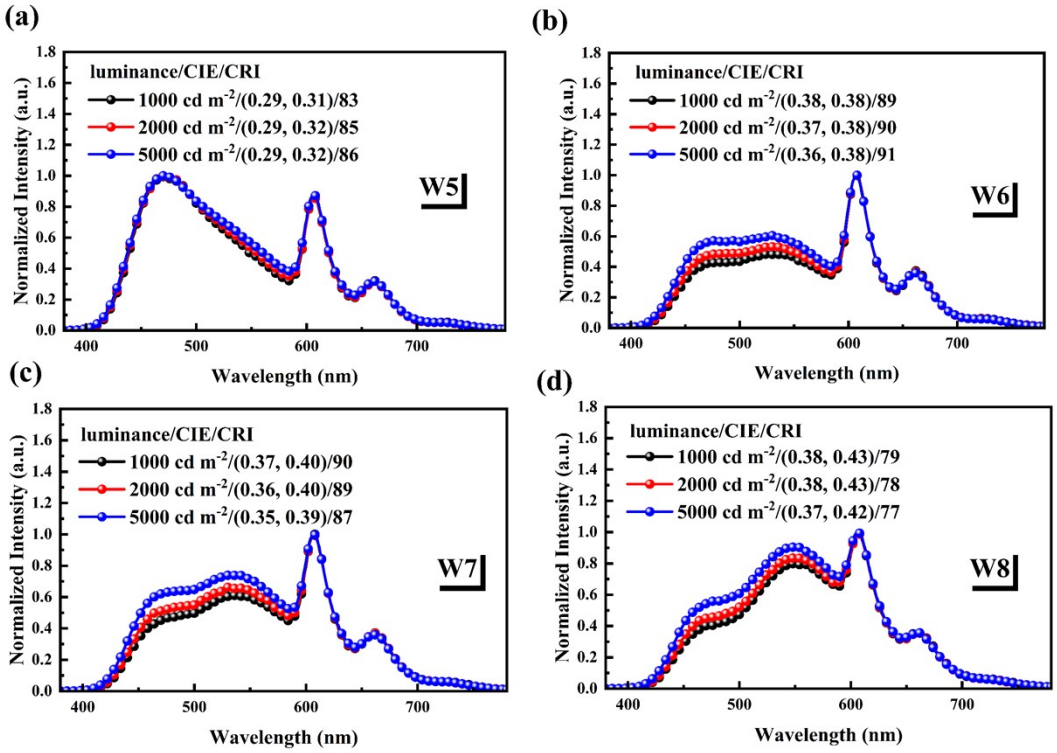

Fig. S13. The normalized EL spectra of (a) W5, (b) W6, (c) W7, and (d) W8 at different luminance.

12. The transient PL decay of films

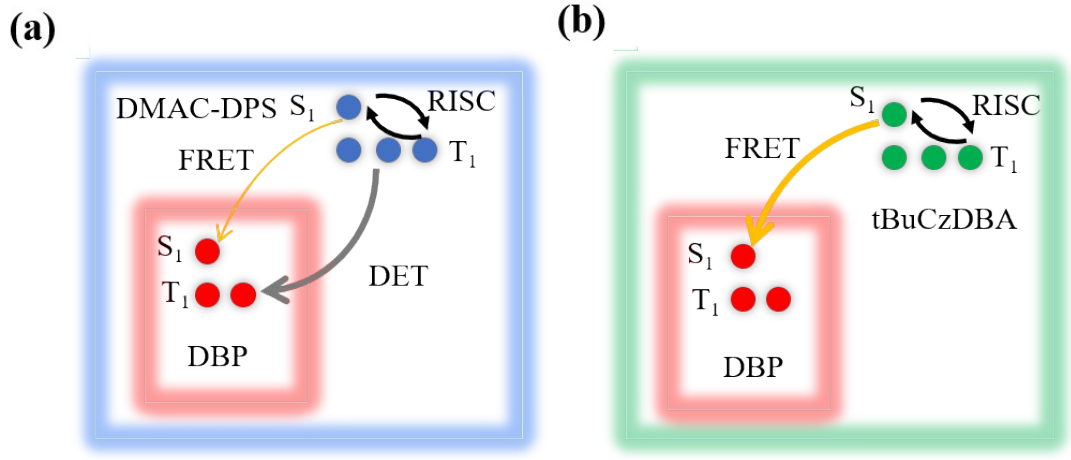

Fig. S14. Exciton energy transfer in film I (a) and film II (b).

13. Absorption and emission spectra of emitters

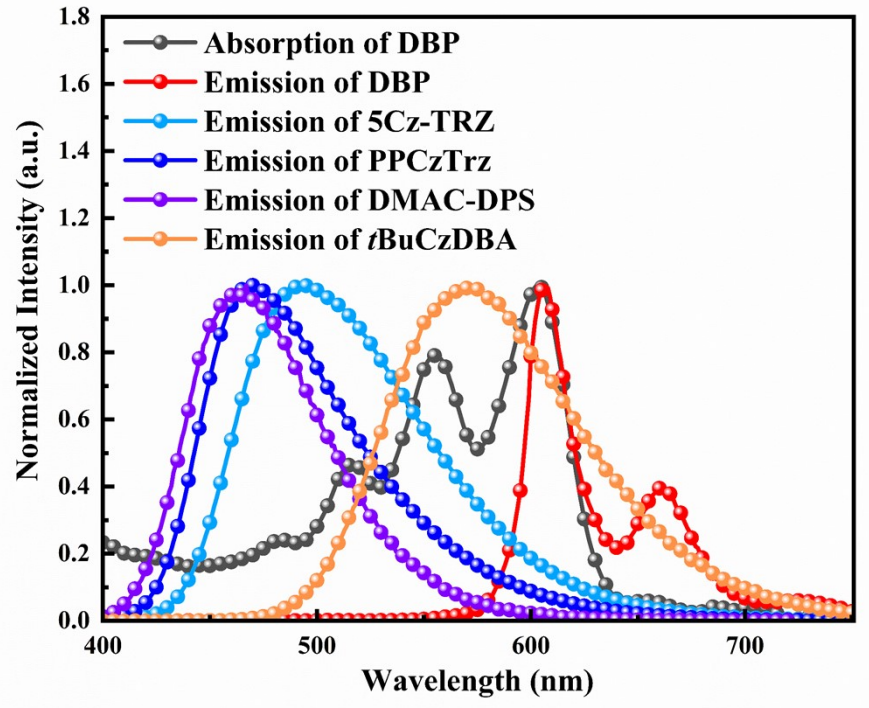

Fig. S15. Absorption of DBP and emissions of *t*BuCzDBA, DMAC-DPS, PPCzTrz, DBP and 5Cz-TRZ.

14. EL performance of device YR

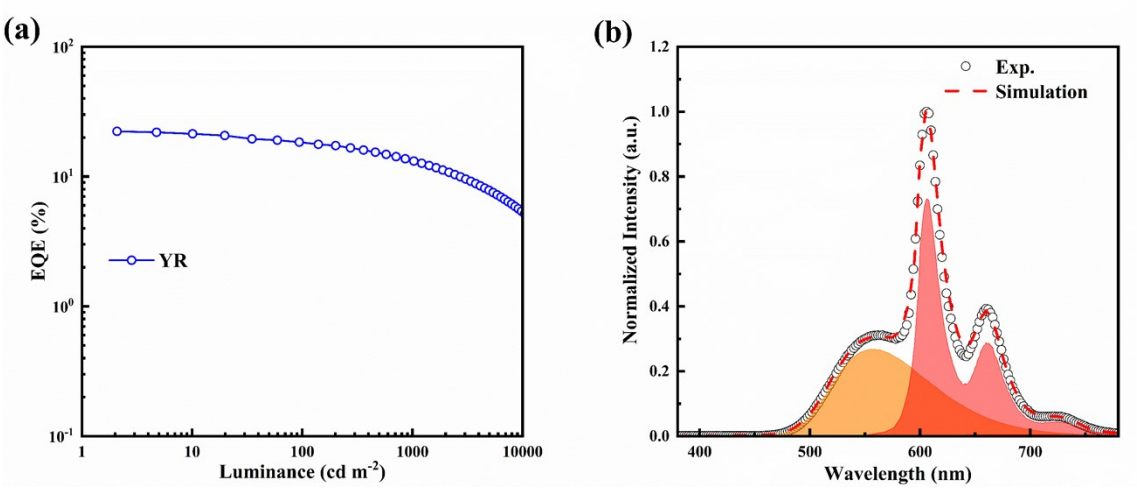

Fig. S16. (a) EQE-luminance curve of TADF-sensitized OLED. (b) EL spectra for device YR.

15. Additional data

Table S1. Summary of previously reported TADF-sensitized all fluorescence WOLEDs.

Ref.	V_{on}[a] (V)	η_{EQE}[b] [%]	η_{CE}[b] [cd A^{-1}]	η_{PE}[b] [lm W^{-1}]	CIE[c]	CRI[c]

W7	2.7	22.4	49.5	55.5	(0.37, 0.40)	90
W11	3.0	30.1	71.3	72.5	(0.42, 0.42)	84
1	2.8	18.2	40.9	44.6	(0.32, 0.39)	82
2	3.4	15.6	31.3	28.9	(0.36, 0.38)	95
3	3.2	12.9	30.5	28.3	(0.42, 0.46)	78
4	2.6	20.5	51.3	59.6	(0.36, 0.41)	72
5	2.5	16.7	/	43.3	(0.44, 0.45)	80
6	2.6	23.0	53.3	64.4	(0.32, 0.41)	74
7	/	21.1	/	43.4	(0.39, 0.41)	83
8	2.6	21.6	48.1	58.1	(0.47, 0.46)	84
9	/	30.7	/	57.7	(0.31, 0.37)	76

[a] At a luminance of 1 cd m^{-2}. [b] Efficiencies of the maximum. [c] At a luminance of 1000 cd m^{-2}.

16. Simulation method and parameters

A classical electromagnetic model was used for the optical simulation of the proposed OLEDs. The emissive exciton was treated as an oscillating (harmonic oscillator) dipole and driven by the reflected electromagnetic field. As OLED is consisted of stacked thin films, the transfer matrix method was utilized for optical calculation. The detailed optical simulation processes were described by Furno et al.[10] The simulation was done in an in-house developed simulation tool. A device architecture Glass/ITO (110 nm)/HTL (x nm)/EML (17.5 nm)/ETL (y nm)/Al (100 nm) was adopted, where the thickness x and y were varied. **Fig. S17** plots the complex refractive indices of all the materials used for simulation. For simplification, the electrical loss is ignored in our simulation.

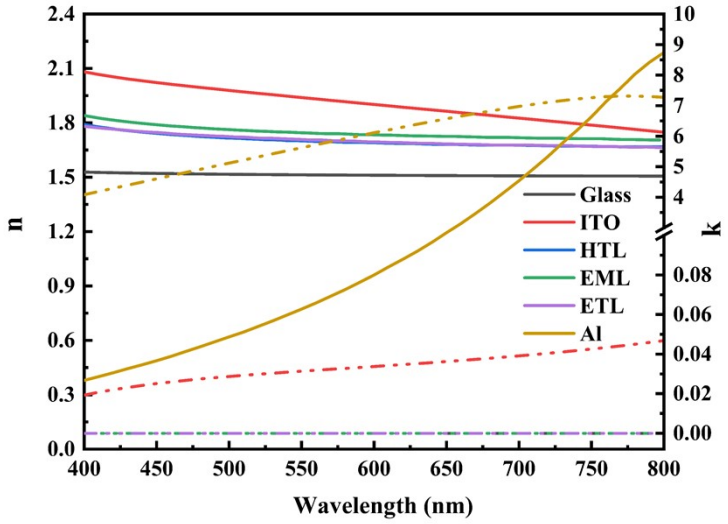

Fig. S17. The complex refractive indices of all the materials used for simulation.

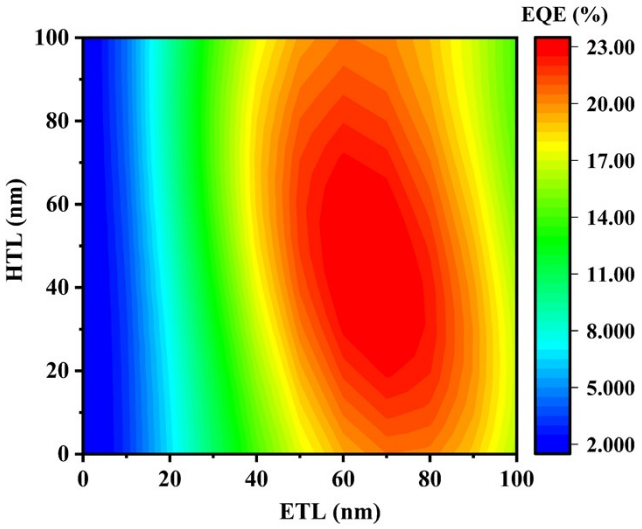

Fig. S18. Calculated optical out-coupling efficiency for blue OLED as a function of the HTL and ETL thicknesses.

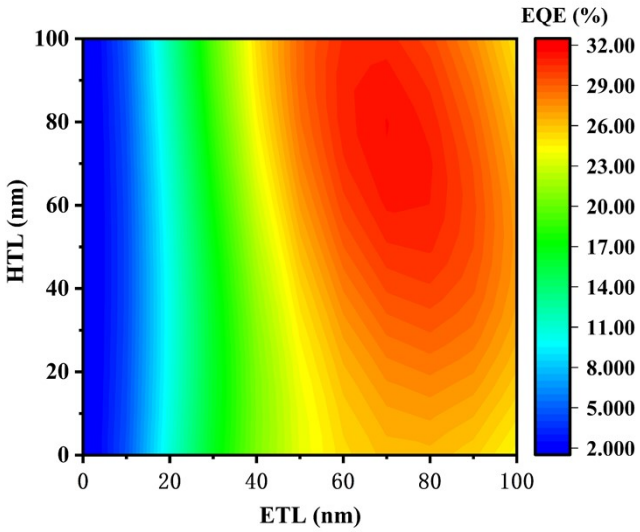

Fig. S19. Calculated optical out-coupling efficiency for yellow OLED as a function of the HTL and ETL thicknesses.

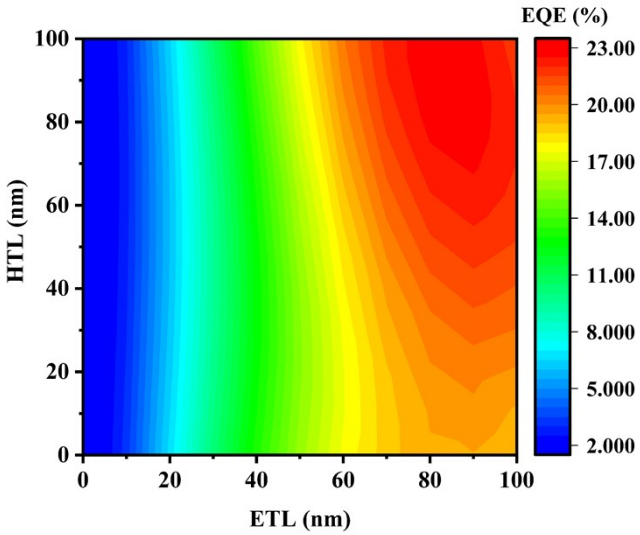

Fig. S20. Calculated optical out-coupling efficiency for red OLED as a function of the HTL and ETL thicknesses.

17. EL performance of device W10 and W11

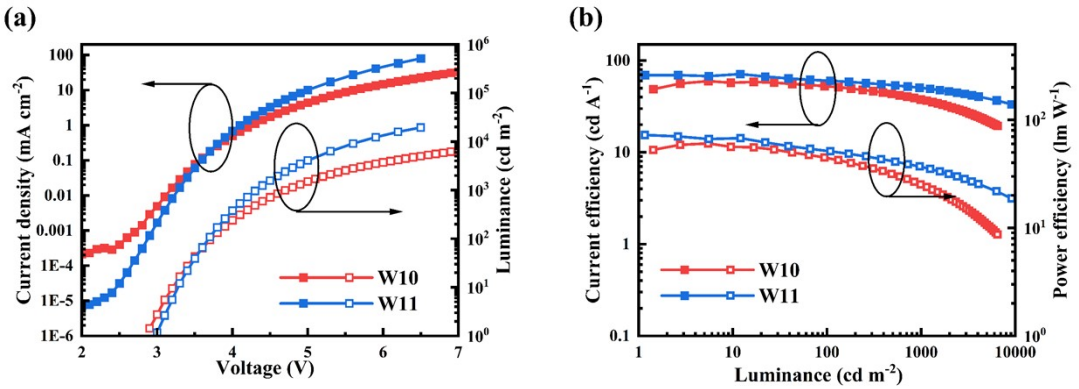

Fig. S21. (a) Current density-voltage-luminance characteristics. (b) CE-luminance-PE curves of W10 and W11.

Device W10: ITO/HAT-CN (5 nm)/TAPC (40 nm)/TCTA (10 nm)/CBP:PPF:*t*BuCzDBA (1:1, 10%, 4 nm)/CBP:PPF:DBP (1:1, 0.5%, 3 nm)/CBP:PPF:*t*BuCzDBA (1:1, 10%, 4.5 nm)/mCBP:PPF:PPCzTrz (1:1, 20%, 6 nm)/PPF (10 nm)/PBPPhen (50 nm)/Liq (2 nm)/Al (100 nm).

Device W11: ITO/HAT-CN (5 nm)/TAPC (40 nm)/TCTA (10 nm)/CBP:PPF:*t*BuCzDBA (1:1, 10%, 4 nm)/CBP:PPF:DBP (1:1, 0.5%, 3 nm)/CBP:PPF:*t*BuCzDBA (1:1, 10%, 4.5 nm)/mCBP:PPF:5Cz-TRZ (1:1, 20%, 6 nm)/PPF (10 nm)/PBPPhen (50 nm)/Liq (2 nm)/Al (100 nm).

18. Lifetime of WOLEDs

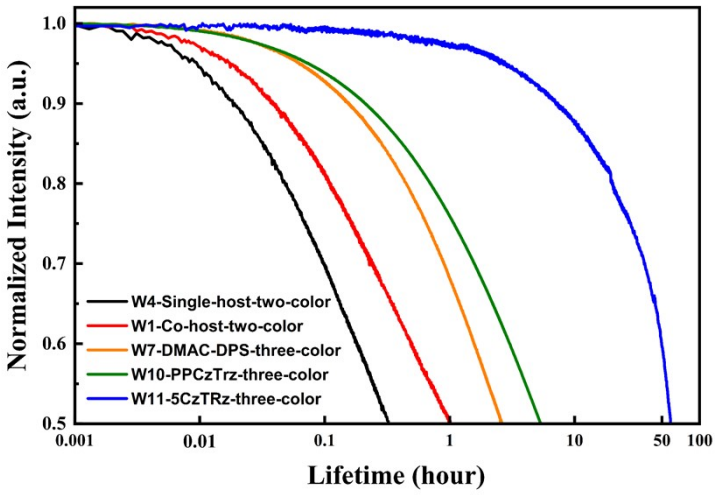

Fig. S22. Device lifetime of two-color and three-color all fluorescence WOLEDs measured at an initial luminance of 3000 cd m^{-2}.

19. References

1. Z. Wu, Q. Wang, L. Yu, J. Chen, X. Qiao, T. Ahamad, S. M. Alshehri, C. Yang, D. Ma, *ACS Appl. Mater. Interfaces*, **2016**, 8, 28780.

2. X. L. Li, G. Xie, M. Liu, D. Chen, X. Cai, J. Peng, Y. Cao, S. J. Su, *Adv. Mater*., **2016**, 28, 4614.

3. Z. Wang, X.-L. Li, Z. Ma, X. Cai, C. Cai, S.-J. Su, *Adv. Funct. Mater*., **2018**, 28, 1706922.

4. Z. Wu, Y. Liu, L. Yu, C. Zhao, D. Yang, X. Qiao, J. Chen, C. Yang, H. Kleemann, K. Leo, D. Ma, *Nat. Commun*., **2019**, 10, 2380.

5. C. Zhang, Y. Lu, Z. Liu, Y. Zhang, X. Wang, D. Zhang, L. Duan, *Adv. Mater*., **2020**, 32, e2004040.

6. H. Liu, J. Chen, Y. Fu, Z. Zhao, B. Z. Tang, *Adv. Funct. Mater*., **2021**, 31, 2103273.

7. X. Hong, D. Zhang, C. Yin, Q. Wang, Y. Zhang, T. Huang, J. Wei, X. Zeng, G. Meng, X. Wang, G. Li, D. Yang, D. Ma, L. Duan, *Chem*, **2022**, 8, 1705.

8. Y. Fu, H. Liu, D. Yang, D. Ma, Z. Zhao, B. Z. Tang, *Adv. Opt. Mater*., **2022**, 10, 2102339.

9. C. Zhang, D. Zhang, Z. Bin, Z. Liu, Y. Zhang, H. Lee, J. H. Kwon, L. Duan, *Adv. Mater*., **2022**, 34, e2103102.

10. M. Furno, R. Meerheim, S. Hofmann, B. Lüssem, K. Leo, *Phys. Rev. B*, **2012**, 85, 115205.